A finite element test of the 2002-2003 Etna eruption

Pulvirenti F. *[,1,2], Aloisi M.[1], De Guidi G.[2], Mattia M.[1] and Monaco C.[2]
[1] Istituto Nazionale di Geofisica e Vulcanologia, Sezione di Catania, Catania, Italy
[2] Dipartimento di Scienze Geologiche, Università di Catania, Catania, Italy
*Corresponding author: fabiopulvirenti@yahoo.it

Abstract: Structural, morphological and ground deformation studies suggest that the eastern flank of Mt. Etna (eastern Sicily) is spreading seaward. Three contrasting models have been proposed: deep-seated spreading, shallow sliding and tectonic block movements.

According to the deep-seated spreading model (Borgia et al., 1992; Rust and Neri, 1996), both the volcanic edifice and its uppermost basement (down to a 5 km depth) are spreading eastwards because of magma inflation processes. Deep sliding wedges would produce a belt of active contractional structures bordering the volcano at the foot of its southern and eastern flanks and deforming Middle Pleistocene sediments. However morpho-structural studies and geomechanical considerations seems to exclude the possibility of thrust faulting induced by magma intrusion (Firth et al., 1996). According to the shallow sliding model (Rasà et al., 1996; Puglisi and Bonforte, 2004), the eastern mobile sector would be dismembered into minor sub-blocks of volcanics, slowly sliding eastwards under their own weight, accommodated by seaward dipping detachment surfaces at different levels within the volcanic edifice or the sedimentary basement. This model is compatible with geomechanical models and is supported by the distribution patterns of the residual between GPS observed and modelled deformations that show the high mobility of eastern and south-eastern flanks with respect to the rest of the volcano. Problematic is the lacking of seismological evidences supporting the occurrence of shallow sliding planes (Patanè et al., 2005).

The geometry and senses of motion of most of the major active features that affect the eastern sector of the volcanic edifice are kinematically compatible and thus appear to have a common tectonic origin (Monaco et al., 1997; 2005). Such striking geometrical affinities suggest that most of the extensional tectonic features of Etna merge together at depth and represent shallow splays of a deep, normal fault zone driven by tectonic separation of the Ionian and Iblean blocks, reactivated during the Quaternary. The tectonic block model is also supported by recent seismological models based on 3D seismic tomography (Patanè et al., 2005; 2006). However, deformation rates obtained by local GPS data and SAR interferometry (Froger et al., 2001; Lundgren et al., 2004; Puglisi and Bonforte 2004; Palano et al., 2007) suggest that rates up to 10 times higher than that obtained by structural morpho-structural estimations and by permanent GPS velocity field along other sector of the incipient regional rift zone, periodically occur. This suggests that local shallow sliding phenomena can be triggered in the eastern slope of Mt. Etna but they must be framed in the morpho-structural setting of the edifice and in the crustal seismological models.

In order to better understand the kinematics of instability processes on eastern flank of Mt. Etna, a numerical simulation has been applied to a specific case history. In fact, through numerical models we are able to explain how the various tectonic structures interact each other and we can get information about the response of the various layers to magmatic intrusions or gravity related processes. In this work we carried out a 3D finite element simulation using the COMSOL MULTIPHYSICS 3.5a software: a test for simulating the 2002-2003 eruption mechanisms.

1. The 2002-2003 eruptive event: a laboratory for testing kinematics of Mt. Etna Eastern flank

The dynamic of eruptive processes can be understood by the analysis of several types of data, acquired before, during and after eruptive events. Among these, GPS data are useful to calculate fault slip rates and to get information about the opening of eruptive fractures. The data recorded by GPS stations are used in inversion analytic models to find which sources could have generated the observed movements. These models are however based on some assumptions (existence of an elastic, homogeneous and isotropic half-space, validity only for little movements respect to the distance between sources and GPS stations, no faulting, any effect related to topography etc.) for which they are different from the real situation. These assumptions don't allow for example to have good information about vertical variations and, consequently, are not able to show what happens under the surface where the source acts. A way to better approach the reality is the finite element method (FEM). In this work we used the finite element software COMSOL MULTIPHYSICS 3.5a to investigate the dynamic processes involved in the 2002-2003 eruption at Mount Etna.

The 2002-2003 eruptive event was a peculiar event in the story of eruptions on Etna. During this event in fact eruption involved two different sectors (north and south) with the emission of two distinct lava flows. Here's a brief description. On the night of 26 October 2002 at 20:25 (GMT) a seismic swarm took place in the central upper part of Mount Etna, some hours later an intense explosive activity with lava effusion and ash columns began at the south flank from a fracture oriented N-S at 2750 m. During the first hours of 27 October, and until 28 October, a long field of eruptive fissures, parallel to the NE Rift, began to propagate radially towards the north-east flank. The

opening of these fractures was accompanied and followed by seismic activity. At the onset of the eruption, the epicentre time pattern showed a northeast-ward migration of earthquakes along the Northeast Rift. From the early morning of 27 October (01.28 GMT), seismicity (depth max = 3.5 km b.s.l.; M_{max} = 3.8) involved the western tip of the WNW-ESE trending Pernicana fault on the north-eastern flank of the volcano, destroying the Piano Provenzana tourist station. Two days after, on the eastern flank, the Timpe fault system has been reactivated with dextral-oblique motion; (/MONACO *et al*, 2005) between San Giovanni Bosco and Santa Venerina (earthquake of 29/10/2002, 10.02 GMT; M=4.4) and in the Guardia village (earthquake of 29/10/2002; 16.39 GMT; M=4) with oblique-dextral motion. The eruption lasted 9 days with emission of lava fluxes and an intense Strombolian activity. The eruption continued on the south flank and ended on January 28, 2003.

The analysis of the deformation pattern and the use of inversion procedures for surface data (Aloisi et al., 2003) indicated that displacements observed can be interpreted as the response of the volcanic edifice to a double dike intrusion: a fast uprise of an eccentric dike triggered the eruption and a lateral intrusion of a second dike at north-east flank that was the principal cause of the deformation observed. The fast rise of the south dike was probably caused by the existence of previous lava conduits, opened during the 2001 south eruption in the same area.

The aim of our work is to reproduce the 2002-2003 eruptive event and to compare the surface displacements calculated numerically with that recorded by GPS stations and already modelled by analytic methods.

2. Model description

The geometry of the model is formed by different layers: the volcano edifice, the clay substrate and the layer including calcarenites and crystalline basement. The topography of the volcano is reproduced using a digital elevation model with a 1000 m resolution. Four tectonic structures have been then inserted: Pernicana fault, Timpe fault system, Trecastagni fault and Acitrezza fault (Fig. 1). Faults are reproduced by contact conditions. All the physical parameters for subdomains and boundaries (including the dikes) have been set with the use of specific functions that reproduce the variation of density, Young modulus or gravitational load conditions from height data. The mesh is formed by about 700 thousand elements and is gradually refined from the bottom to the top of the computational domain to get more accurate values at volcano surface. The execution of the model is instead divided in two parts: first of all the execution of a *moving mesh* module that generates the topology of the volcanic edifice, then the execution of structural mechanics with a particular parametric solver (Fig. 2). Using particular settings, the parameter (*para*) grows up from the value 0 to 2. From 0 to 1, a step by step procedure makes the gravitational load growing up linearly until it reaches 100%. Then, from para=1 to para=2, the gravitational load is maintained to its 100 percent and prescribed movements (opening and shear components for the dikes) are gradually applied until the maximum value is reached. The surface movements we got have been compared to recorded and analytical data.

2.1 Phase I: Geometry creation and subdomain settings

To better reproduce all the features existing on Etna Mount a complex model has been constructed. It takes into account the presence of the volcanic edifice, of the lithostratigraphic units under the volcano surface, of the east flank principal fault systems and of gravitational load conditions.
The computational domain size is 36x41x10 km (fig 1). Using the *workplane* and extrusion procedures it has been divided in subdomains, grouped by physics characteristics to obtain 2 principal groups: the first group depth is – 3 km b.s.l.(our zero), the second group depth is from -3 km to -10 km b.s.l. Hereafter we identify these two groups as group 1 and 2 respectively.

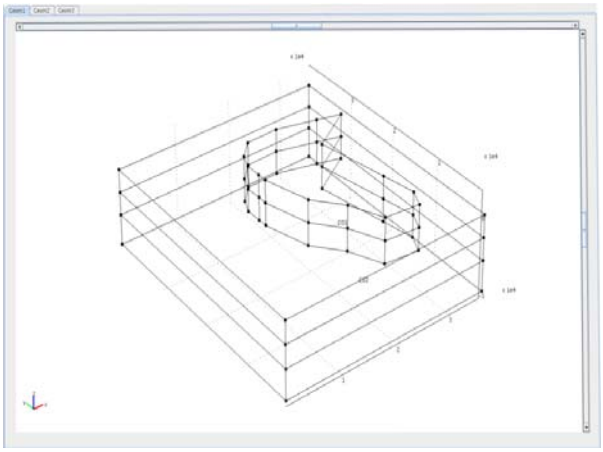

Figure 1. Geometry for 2002 Etna eruption. The computational domain is divided in subdomains having different depth and grouped by physical characteristics.

The surface of group 1 is the layer on which the volcanic edifice is formed; to make it, we have to import a DEM (Digital Elevation Model) file, that is a text file with 3 columns containing the x, y and z coordinates of some points of the volcano surface. In our case the DEM file (STRM data), has a 1000 m resolution and is then formed by 36x41 points. The DEM file is imported in COMSOL and the data are read using the *moving mesh* procedure. To make this we inserted the expression :

$$quota(Y,X)*(1+Z/3000) \quad \textbf{(1)}$$

as a prescribed displacement in the moving mesh settings for group 1, where quota (Y,X) is the function referred to DEM file data in the layer reference system XYZ. By this expression, all the points having Z=0 (on sea level) are elevated of a quantity z congruent with DEM data, the points with Z= – 3 km are not elevated and finally the points with Z between 0 and -3 km are

elevated in a way that follow the expression (1). All the points belonging to the group number 2 are instead set as *No displacement*. By this settings the volcano edifice can so be created.

Basing on geological profiles (Monaco et al., 2008) we know about the existence of a clay substrate inside the volcano; its upper surface has a nearly gaussian profile reaching an height of 1250 m under the central craters zone and minor heights elsewhere, with some superficial outcrops. The substrate creation is made choosing some points for which the height of the clay is noted. Importing the file containing the coordinates of these points in COMSOL an interpolation surface can be generated. We called the function for this surface argilla(x,y) and inserted it in the subdomain settings through the following expression:

(z>=argilla(x,y))*(30e9[Pa])+(z>=-1000&&z<argilla(x,y))*(10e9[Pa])+(z<-1000)*(40e9[Pa]) **(2)**

By this expression, all the points having a coordinate z greater than argilla (x,y) are over the clay surface and are set with a Young's modulus of 30 GPa (volcanic products), all the points between argilla (x,y) and – 1 km (b.s.l.) are in the clay substrate and have a Young's modulus of 10 GPa, and all the remaining points, from -1 km to – 10 km (calcarenites and cristallyne basement), are set with a 40 GPa Young's modulus. In this way, we set the lithilogical properties of the different layers. It should be noticed that the Young values used are mean values because it's impossible to consider all the differences between the several rock stratifications present on Etna Mount and, in any case, it will complicate the model with no great variations on results. Other subdomain settings are: Poisson's rate, that is set to 0.25 for all layers, and density. In our model density is 2800 kg/m^3 for volcanic products , 1900 kg/m^3 for clay substrate and 2600 kg/m^3 for calcarenites and crystalline basement.

2.2 Phase II: Boundary settings and fault planes creation

In this phase we chose all the constrain conditions for internal or perimetric surfaces of our computational domain. We applied the condition *fixed* to the domain base and the condition *roller* to the domain perimeter. The internal part of our domain is instead formed by several boundaries that have been generated during the creation of geometry. Some of these boundaries correspond to the dikes and some other to the fault planes. To create all these boundaries we used the work plane to put some particular points in the domain surface, then we connected them and formed a structure that is extruded and integrated in the domain. In this way some of its perimetric boundaries correspond to the positions of the principal fault systems, other perimetric boundaries to the positions of the 2002 eruption dikes (as inferred from analytical model) (fig 2). Working with the *assembly* the program identifies the internal and external boundaries of the structure we created. Its perimetric boundaries become so couples of faces in contact and we can apply normal or tangential prescribed movements on them.

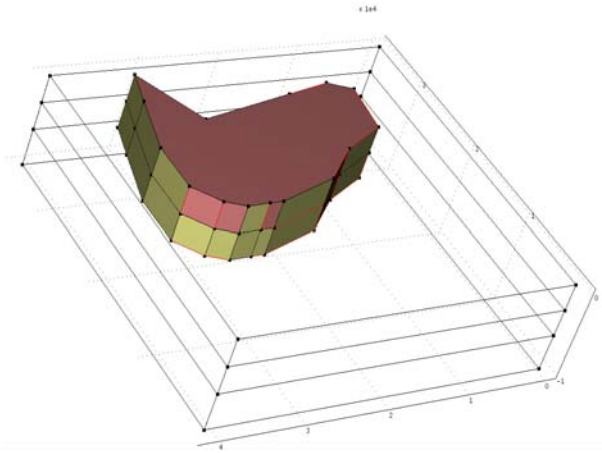

Figure 2. Boundaries creation. The connection of particular points on the volcano surface can be used to form a structure that contains dikes and faults.

The north dike (6 km long and 2 km deep) is composed by two couples of faces: each face of the first couple is 2.5 km long and has a 0.5 m opening component assigned, each face of the second couple is 3.5 km long and has the same opening component but a tangential component (left lateral strike-slip) of 0.25 m also. The expressions for these movements are inserted in the boundary settings area and are respectively:

-((z>=-2000)*(spost)+(z<-2000)*(spost1))*ampli **(3)**

and

((z>=-2000)*(spost2)+(z<-2000)*(spost1))*ampli **(4)**

where *spost*, *spost1* and *spost2* are constants with values 0.5, 0 and 0.25 respectively, and *ampli* is a parametric function defined as:

(para>1)*(-1+para) **(5)**

The use of ampli function is necessary to apply these movements only for some values of the parameter para, as we see better further.

Each face for the south dike is 1.6 km long and 2.5 km deep. The expression used for this dike is:

-((z>=-500)*(spost)+(z<-500)*(spost1))*ampli **(6)**

The minus sign appearing in (3) and (6) indicates that the movement is applied to the outgoing normal. By expressions (3) and (4) the north dike movement is applied from its top (corresponding to the volcano surface) to a depth of – 2 km b.s.l., while, by (6), the south dike the movement is applied from the top to – 500 m depth; out of these values the movement is zero.

The faults we inserted belong to the eastern flank and are: Pernicana, Timpe, Tracastagni and Acitrezza. We chose these faults because all the data recorded by

GPS stations show that they are the principal systems involved in the accommodation of the eastern flank movements. The fault planes position has been inferred from geological and structural data available in literature and directly mapped in the field, the fault planes depth has been established from earthquakes hypocentral distribution (Patanè et al., 2005) and, on this basis, a depth of – 6 km is assigned to Timpe and Trecastagni fault planes and a –3 km depth is assigned to Pernicana and Acitrezza fault planes. To reproduce the movements knew for these fault planes, the corresponding boundaries are set as master and slave of *contact pairs* (fig.3). In this condition pairs have an initial contact pressure and can separate or slide each other but no compenetration is possible. The remaining perimetric boundaries are set as *identity* condition.

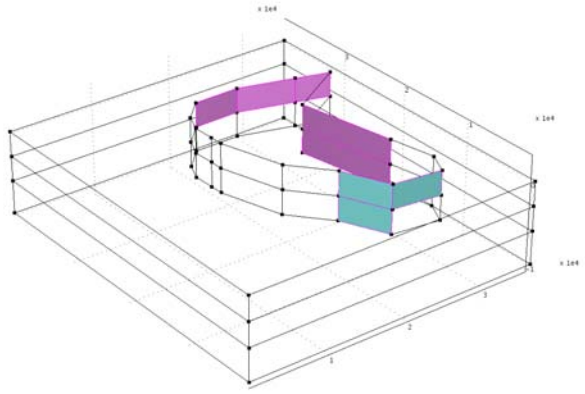

Figure 3. Contact pairs created to simulate the faults. From north to south, Pernicana, Timpe, Trecastagni and Acitrezza faults. Light-blue are master surfaces and purple the slave ones.

All the other internal boundaries of the computational domain, the volcano surface also, are set as *free*. After subdomains and boundaries are set, the mesh has been created. In this case we chose to refine the mesh at surface while it is coarser in depth(z<-3 km). In particular the maximum element size is 1500 for -10 km<z<-6 km, 1000 for -6km<z<-3 km and 500 from z> -3 km to the volcano surface (fig. 4).

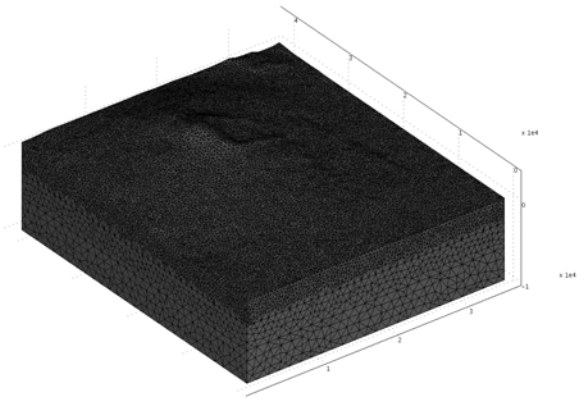

Extended mesh:	
Number of degrees of freedom:	427261
Base mesh:	
Number of mesh points:	141929
Number of elements:	781543
Tetrahedral:	781543
Prism:	0
Hexahedral:	0
Number of boundary elements:	70419
Triangular:	70419
Quadrilateral:	0
Number of edge elements:	2060
Number of vertex elements:	106
Minimum element quality:	0.2535
Element volume ratio:	0.0028

Figure 4. The mesh is composed by linear lagrangian tetrahedrical elements and is fine where a better results is required (volcano surface). The number of degrees of freedom is about 400 thousand with a minimum element quality of about 0.25.

2.3 Phase III: Solving settings

To solve the model we chose a parametric solver instead of a stationary one. We defined the parameter *para*, which goes from 0 to 2 with a step of 0.1 For 0<para<1 the gravitational load is applied. The gravitational load application can be applied in the subdomain settings as the volume force Fz in the z negative direction. The expression used is:

-((z>=argilla(x,y))*(2800[kg/m^3])+(z>=-1000&&z<argilla(x,y))*(1900[kg/m^3])+(z<-1000)*(2600[kg/m^3]))*9.81[m/s^2]*ampli2 **(7)**

This expression depends on the height values z and is the product of the density of each layer for the gravitational acceleration and for another parametric function, *ampli2*, that is defined in the Boundary Expression settings as:

(para<=1)*para+(para>1) **(8)**

Using the expression (7) the gravitational load is gradually applied when para is <1 and is maintained to its 100% for 1<para<2.

By expression (5), when para is major than 1 the prescribed displacements of the dikes are applied also. The application of the prescribed displacements is gradual, it reaches the maximum value when the simulation over at para =2.

2.4 Phase IV: Solving

To solve the model we execute, first of all, the moving mesh with a stationary solver. After the volcano has been generated the solution is stored and the structural mechanics is solved with a parametric solver (PARDISO). Figure 5 show the result of the moving mesh process.

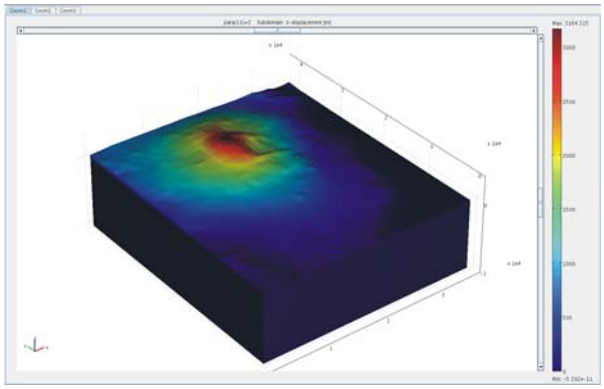

Figure 5. Volcano surface generation by moving mesh.

3. Postprocessing and results

The results can be visualized in the postprocessing area. We are interested to know the x,y and z values of the movements triggered by the dikes at the volcano surface. To get, for example, x values we must plot the expression:

u-with(11,u) (**10**)

where u is the variable for represent x displacements, the value 11 correspond to the eleventh step of para (para=1) when the maximum value of gravitational load application is reached and *with* is a special function to subtract the gravitational load. The abrupt gravitational load application leads in fact to an overall lowering of the volcano and of the other layers that doesn't exist in the real situation whereas the gravitational load has been applied during thousands of years until the present equilibrium state. So our system must be re-equilibrated and this can be made by the *with* function. To plot the y and z components it is sufficient to substitute the respective variables v and w in the expression (10).

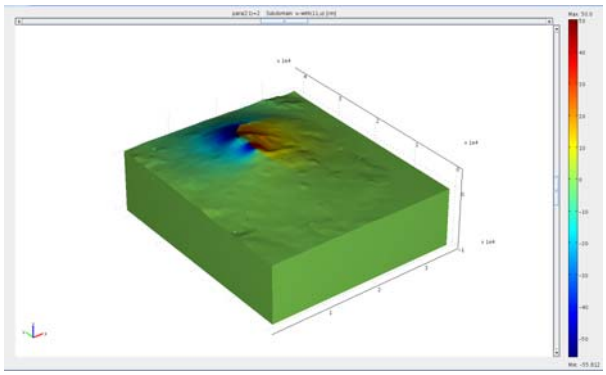

Figure 6. x surface displacements.

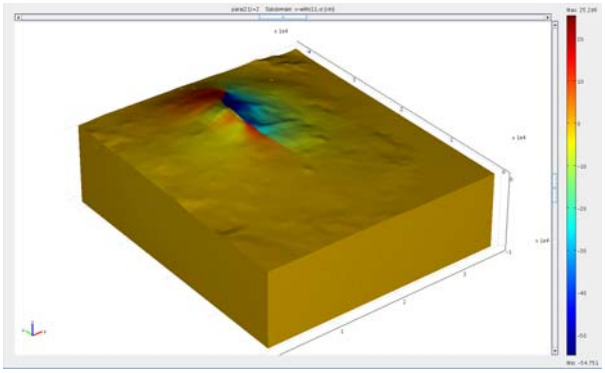

Figure 7. y surface displacements.

From x and y displacements we calculated the displacement vectors at GPS station positions and compared them with the vectors obtained by recorded data and by analytic procedures.

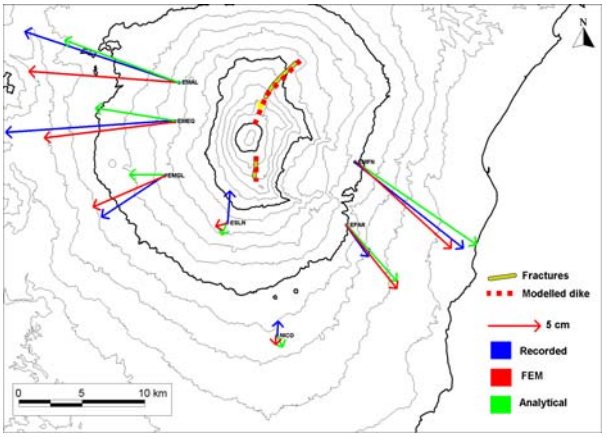

Figure 8. Comparison between displacement vectors estimated from recorded, numerical, and analytical data.

As can be seen in figure 8, FEM vectors have a good general agreement with recorded ones apart from the stations of Serra La Nave (ESLN), Nicolosi (NICO) and Monte Maletto (EMAL) that have a similar modulus but different directions. At Monte Farelle (EFAR) instead the directions are very similar but the modulus of FEM and analytical vectors are double respect to recorded one. Finally figure 9 shows the results for vertical variations.

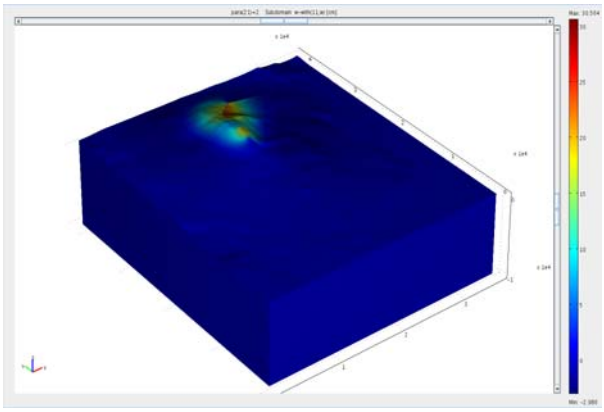

Figure 9. Vertical surface variations.

In figure 10 is showed the comparison between recorded vertical variations and analytical and numerical ones.

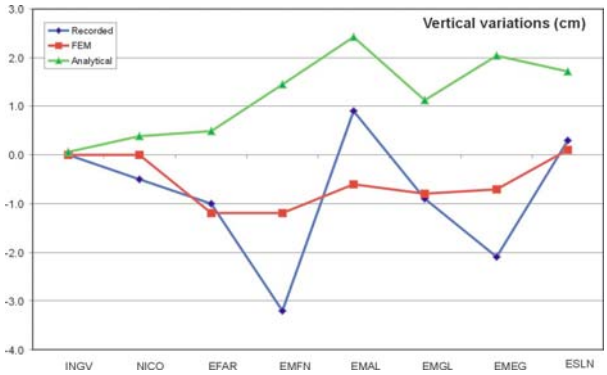

Figure 10. Comparison between recorded, FEM and analytical vertical variations.

As can be seen from figure 10, FEM is better than analytical approach in explaining vertical variations in almost all stations. It is able in fact to compute also negative vertical variations whereas analytical approach gives positive values only. The only difference is at EMAL where FEM gives a negative value respect to the positive value recorded.

4. Displacement along the faults

Numerical model is able to provide a lot of information respect to analytical model. In particular, the presence of the faults permits to investigate the displacement near them.

4.1 Pernicana fault

x and y displacement along Pernicana Fault results in a left lateral strike slip. Referring to the south side of the fault, x displacements are about 20 cm in the west part with a N135E orientation and gradually rotate to N100E (parallel to the fault plane) and reduces to 5 cm in the most east part. Vertical variations show a normal dip slip in the most west part of about 20 cm. It goes rapidly to zero proceeding eastwards.

4.2 Timpe fault system

At Timpe faults x vector displacements on the west side show a left lateral strike slip: from 4 cm in the north part with an orientation of about N135E, they gradually rotate to N180E, aligning with the fault, and contemporaneously reducing to 2 cm. On the east side, instead, the vectors in the north part are oriented N90E and have a modulus of 3 cm rapidly going to zero in the south part. y displacements are about 3 cm at the north west side with vectors oriented N120E. Moving towards south in the west part, the movement gradually reduces to 1 cm and vectors change their orientation as for x displacements. On the north-east side y displacement is 1 cm and gradually goes to zero. Vertical variation shows a lowering on the west side and an uplift on the east side. The lowering goes from -2 cm in the north part to -0.5 in the south part. The uplift is instead about 0.7 cm in the north part and gradually goes to zero towards south.

4.3 Trecastagni fault

x displacements on Trecastagni fault shows respectively a displacement of about 0.3 cm on the north-east side going to 0.1 in at south-east while it is about zero on the west side. y displacements show a right lateral strike slip of about 1 cm. z displacement show a lowering on the east side going from 0.2 cm in the north part to 0.1 cm in the south part.

4.4 Acitrezza fault

x displacements show a right lateral strike slip of 0.2 cm while y displacements a compression of about 0.7 in the west part to 0.3 cm going eastwards. The z displacements show a lowering in the north part of about 0.02 cm and an uplift at south of about 0.08 cm.

5. Conclusions

Our test shows that FEM provides more information than analytical models. The presence of the faults permits in fact to investigate the displacements near them. The general FEM data fit is good and we have a reduced chi-squared X^2 equal to 1.0 considering an a-posteriori standard deviation of 0.018 m for the horizontal and vertical displacements. Otherwise with the same standard deviation the analytical model is not able to pass the reduced chi-square test; to pass it, the a-posteriori standard deviation must be 0.030 m. Moreover, FEM explains well the vertical variations, even where they are negative, with the only exception of EMAL; analytical vertical variations are instead ever positive.

The reason for these differences is clear: the use of finite elements permits to overcome the strong limitations of the analytical model as the use a simple tabular dislocation model [Okada, 1985] in a simple

elastic half-space without heterogeneity, faulting and gravitational load conditions. Adding all these conditions permits to better reproduce the real situation. Naturally our FEM model is not completely detached from analytical model because the dikes are still reproduced as simple rectangular cracks as suggested from analytical inversion model; this is why the uncertainty (standard deviation) is still more than the instrumental error and we cannot completely explain the data as observed. The final aim is so to construct a model that can explain well all surface displacements to reproduce the deformative GPS pattern before, during and after eruptive critical events.

6. References

Bianchi F; Carbone S; Grasso M; Invernizzi G; Lentini F; Longaretti G; Merlini S; Mostardini F; Sicilia orientale: profilo geologico Nebrodi-Iblei Memorie della Societa Geologica Italiana, volume: 38, anno: 1987, pagine: 429 – 458.

Borgia, A., Ferrari, L., Pasquarè, G., 1992. Importance of gravitational spreading in the tectonic and volcanic evolution of Mount Etna. Nature, 357, 231-235.

Firth, C., Stewart, I., McGuire, W.M., Kershaw, S., Vita-Finzi, C., 1996. Coastal elevation changes in eastern Sicily: implications for volcano instability at Mount Etna. In: McGuire, W.M., Jones, A.P., Neuberg, J. (Eds.), Volcano Instability on the Earth and Other Planets. Geological Society, London, Special Publication, 110, 153–167.

Froger, J.-L., Merle, O., Briole P., 2001. Active spreading and regional extension at Mount Etna imaged by SAR interferometry. Earth and Planetary Science Letters, 148, 245-258.

Lundgren P., Casu F., Manzo M., Pepe A., Berardino P., Sansosti E. and Lanari R.; 2004: Gravity and magma induced spreading of Mount Etna volcano revealed by satellite radar interferometry. Geophys. Res. Lett., 31, doi:10.1029/2003GL018736.

Monaco, C., Tapponnier, P., Tortorici, L. and Gillot, P.Y., 1997. Late Quaternary slip rates on the Acireale-Piedimonte normal faults and tectonic origin of Mt. Etna (Sicily). Earth Planet. Sci. Lett. 147, 125-139.

Monaco C., Catalano S., Cocina O., De Guidi G., Ferlito C., Gresta S., Musumeci C. and Tortorici L. (2005) - Tectonic control on the eruptive dynamics at Mt. Etna volcano (eastern Sicily) during the 2001 and 2002-2003 eruptions. J. Volc. Geoterm. Res., 144, 221-233.

C.Monaco, G.DeGuidi, S.Catalano, C.Ferlito, G.Tortorici e L. Tortorici CARTA MORFOTETTONICA DEL MONTE ETNA Dipartimento di Scienze Geologiche-Università di Catania. Stampa con i fondi INGV-DPC (Progetti 2005-2007, Resp: C. Monaco).

Palano, M., Puglisi, G., Gresta, S., 2007. Ground deformation at Mt. Etna: a joint interpretation of GPS and InSAR data from 1993 to 2000. Bollettino di Geofisica Teorica ed Applicata, 48 (2), 81-98.

Rasa`, R., Azzaro, R., Leonardi, O., 1996. Aseismic creep on faults and flank instability at Mount Etna volcano, Sicily. In: McGuire, W.C., Jones, A.P., Neuberg, J. (Eds.), Volcano Instability on the Earth and Other Planets. Geological Society, London, Special Publication, 110, 179– 192.

Okada, Y., Surface deformation due to shear and tensile faults in half-space,
Bull. Seismol. Soc. Am., 75, 1135– 1154, 1985.

Patane`, D., Mattia, M., Aloisi M., 2005. Shallow intrusive processes during 2002–2004 and current volcanic activity on Mt. Etna. Geophysical Research Letters, 32, L06302, doi:10.1029/2004GL021773, 2005

Patane`, D., Barberi, G., Cocina, O., De Gori, P., Chiarabba, C., 2006. Time-resolved seismic tomography detects magma intrusions at Mount Etna. Science, 313, 821-823.

Puglisi, G., Bonforte A., 2004. Dynamics of Mount Etna Volcano inferred from static and kinematic GPS measurements. Journal Of Geophysical Research, 109, B11404, doi:10.1029/2003JB002878, 2004

Rust, D., Neri, M., 1996. The boundaries of large-scale collapse on the flanks of Mount Etna, Sicily. In: McGuire, W.J., Jones, A.P., Neuberg, J. (Eds.), Volcano Instability on the Earth and Other Planets. Geological Society, London, Special Publication, 110, 193– 208.

7. Acknowledgements

We thank GianLuigi Zanotelli, Valerio Marra and Remi Magnard for their support and useful suggestions.